ADVANCED MATERIALS
www.advmat.de

www.MaterialsViews.com

Highly Photoactive, Low Bandgap TiO_2 Nanoparticles Wrapped by Graphene

*Joon Seok Lee, Kyeong Hwan You, and Chan Beum Park**

Photocatalytic materials have long been studied to alleviate the deterioration of natural environments created by toxic pollutants and the exhaustion of energy resources by splitting water for hydrogen production utilizing light energy.[1–4] Titanium dioxide (TiO_2), an oxide semiconductor, is regarded as a suitable material for various photocatalytic applications because of its strong oxidizing power, high chemical inertness, low cost, and long-term stability.[5] However, a large bandgap (3.2 eV) of anatase TiO_2 restricts its use only to the narrow light-response range of ultraviolet (only about 3–5% of total sunlight).[6] On the other hand, two-dimensional nanomaterials have recently received high attention from materials scientists because of their unique properties. In particular, graphene nanosheets, a monolayer of carbon atoms arranged in a honeycomb network, exhibit superior electrical conductivity, excellent mechanical flexibility, large surface area, and high thermal/chemical stabilities.[7–12] When graphene is hybridized with other materials, graphene can slow the recombination of photo- or electro-chemically generated electron-hole pairs, increasing charge transfer rate of electrons and surface-adsorbed amount of chemical molecules through π–π interactions.[13–16]

Herein we report on the synthesis of graphene-wrapped anatase TiO_2 nanoparticles (NPs) that highly enhance the photocatalytic activity of TiO_2 under visible light irradiation. We have prepared graphene-anatase TiO_2 hybrid NPs by wrapping amorphous TiO_2 NPs with graphene oxide (GO), followed by a *one-step* GO reduction and TiO_2 crystallization via hydrothermal treatment (**Figure 1**A). Uniform, amorphous TiO_2 NPs with an average diameter of 500 nm were obtained through a sol-gel process with the modification of NP surface to have amine functional groups by 3-aminopropyltriethoxysilane (Figure 1B). We created GO-wrapped amorphous TiO_2 NPs by co-assembly of positively charged TiO_2 NPs with negatively charged GO nanosheets (Figure 1C). GO was prepared by the oxidation of graphite. According to our AFM analysis, the height of bare GO nanosheets was approximately 1.2 nm (Figure S1). The SEM image in Figure 1C indicates that bare amorphous TiO_2 NPs were entirely wrapped by GO nanosheets. After hydrothermal treatment for the reduction of GO and the crystallization of amorphous TiO_2 NPs, the dense precursors turned into porous nanospheres having a hierarchical structure that consisted of interconnected nanocrystals with intact graphene nanosheets (Figure 1D). To observe the effect of carbon content in the hybrid materials, we wrapped TiO_2 NPs with GO nanosheets by using different weight ratio of GO to TiO_2 NPs (0:1, 0.0025:1, 0.005:1, 0.02:1, and 0.05:1). The SEM images in Figure S2A show that the coverage of graphene sheet on TiO_2 NPs was highly affected by the carbon content; TiO_2 NPs were entirely wrapped by graphene in the weight ratios of 0.02:1 and 0.05:1 (GO: TiO_2). Note that the color of graphene-TiO_2 NPs became much darker with the increasing amount of GO in the hybrid materials (Figure S2B). According to our elemental analysis, carbon content in the graphene-TiO_2 NPs gradually increased from 0 to 4.22 wt% with the increasing GO content (Table S1).

We conducted TEM, XRD, and Raman analyses on graphene-wrapped TiO_2 NPs. The high-resolution TEM image in **Figure 2**A shows few-layered graphene nanosheets and a well-defined crystallinity of TiO_2 with a lattice spacing of 0.35 nm, which is assigned to the (101) plane of anatase. It was difficult to precisely control the number of graphene layers on the TiO_2 NPs even with the change of GO content in the hybrid materials (Figure S3). XRD patterns of bare amorphous TiO_2 NPs, GO-TiO_2 NPs, and graphene-TiO_2 NPs are shown in Figure 2B; no peak was observed in the XRD patterns of bare amorphous TiO_2 NPs and GO-TiO_2 NPs, indicating that the pre-formed TiO_2 NPs were amorphous, while all the identified peaks for graphene-TiO_2 NPs were assigned to anatase (JCPDS, no. 21-1272). Note that a broad diffraction peak at around 26° corresponding to graphene was not observed in the XRD pattern of graphene-TiO_2 NPs due to the strong intensities of diffraction peaks from crystalline TiO_2 NPs. Figure S4 shows the Raman spectrum of graphene-TiO_2 NPs. Raman lines at 153, 393, 516, and 634 cm^{-1} were assigned to the E_g, B_{1g}, A_{1g} or B_{1g}, and E_g modes of anatase phase, respectively (Figure S4A).[17] The Raman bands at 1344 and 1586 cm^{-1} were assigned to the D line (breathing mode of k-point phonons of A1g symmetry) and the G line (the first-order scattering of the E2g phonons), respectively.[18] Hydrothermal treatment resulted in a slight increase of the D/G intensity ratio from 0.7 for GO in GO-TiO_2 NPs to 0.95 for graphene in graphene-TiO_2 NPs, which is attributed to the formation of new and smaller sp^2 domains during the treatment (Figure S4B).

We investigated optical diffusion reflection spectra of graphene-TiO_2 NPs. For comparison, we prepared different hybrid materials made of graphene and TiO_2 NPs by wrapping GO nanosheets on *crystalline* anatase TiO_2 NPs, not *amorphous* TiO_2 NPs, and then reducing GO to graphene. For convenience, we denote this hybrid material as "graphene-TiO_2 NPs (*two-step* hydrothermal)" to distinguish them from "graphene-TiO_2 NPs" that were prepared by *one-step* TiO_2 crystallization and GO

J. S. Lee,[+] K. H. You,[+] Prof. C. B. Park
Department of Materials Science and Engineering
Korea Advanced Institute of Science
and Technology (KAIST), 335 Science Road,
Daejeon 305-701, Republic of Korea
E-mail: parkcb@kaist.ac.kr
[+] These authors contributed equally to this work.

DOI: 10.1002/adma.201104110

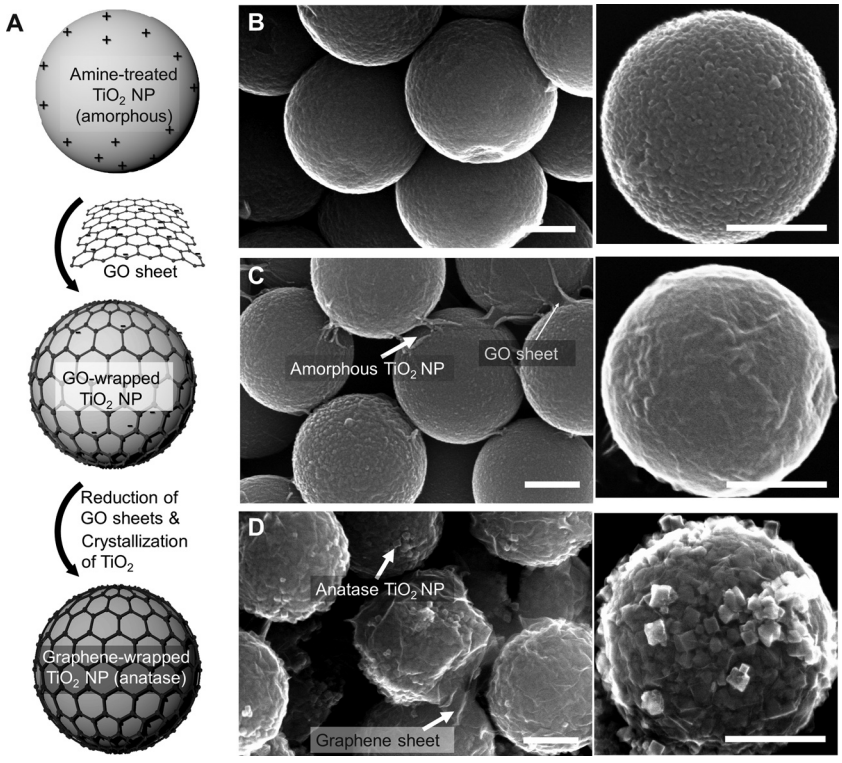

Figure 1. Schematic illustration of synthesis steps for graphene-wrapped anatase TiO_2 NPs and corresponding SEM images. (A) Synthesis steps of graphene-wrapped TiO_2 NPs; the surface of amorphous TiO_2 NPs was modified by APTMS and then wrapped by graphene oxide (GO) nanosheets via electrostatic interaction. Graphene-wrapped anatase TiO_2 NP was synthesized through *one-step* hydrothermal GO reduction and TiO_2 crystallization. (B) SEM images of bare, amorphous TiO_2 NPs prepared by sol-gel method. (C) SEM images of GO-wrapped amorphous TiO_2 NPs. The weight ratio of GO to TiO_2 was 0.02:1. (D) SEM images of graphene-wrapped anatase TiO_2 NPs. Scale bar: 200 nm.

reduction as explained earlier. **Figure 3**A shows the UV-visible spectra of graphene-TiO_2 NPs, graphene-TiO_2 NPs (*two-step* hydrothermal), and bare anatase TiO_2 NPs. We observed a red-shift in the absorption edge and a strong absorption in the visible light range for both graphene-TiO_2 NPs and graphene-TiO_2 NPs (*two-step* hydrothermal). The inset in Figure 3A shows plots of the Kubelka-Munk remission function (i.e., relationship of $[\alpha h\nu]^{1/2}$ versus photon energy) corresponding to each spectrum, which indicates that the bandgap of bare anatase TiO_2 NPs was 3.27 eV, the same as the reported Eg value for anatase TiO_2.[19] While the bandgap of graphene-TiO_2 NPs (*two-step* hydrothermal) estimated from the spectrum was 3.19 eV, the bandgap of graphene-TiO_2 NPs was significantly reduced to 2.80 eV. This phenomenon should occur due to the direct interaction between C and Ti atoms on the NP surface during hydrothermal treatment. According to the literature,[20] Ti atoms rearrange to an octahedral structure when converted from amorphous TiO_2 to crystalline TiO_2. During the heat treatment of GO-TiO_2 NPs, Ti atoms in the amorphous phase should interact more actively with GO than in the crystallized phase in GO/TiO_2 NPs. On the other hand, functional groups on the surface of GO (e.g., -OH, -COOH) disappear when GO is reduced to graphene and the π electrons of C atom cannot bond with others to form a delocalized large π bond.[21] Thus, the remaining unpaired π electrons should easily bond with *more free* Ti atoms on the surface of TiO_2 during the phase transformation from the amorphous TiO_2 in the graphene-TiO_2 NPs. In a similar way to the effect of surface doping that allows the energy level change of conduction (or balance) band,[22] the interaction between unpaired π electrons and Ti atoms during *one-step* crystallization and reduction should result in the shift of the band-edge and the significant reduction of the bandgap of graphene-TiO_2 NPs.

We further measured photocurrents of bare anatase TiO_2 NPs, graphene-TiO_2 NPs (*two-step* hydrothermal), and graphene-TiO_2 NPs by depositing each material on ITO electrodes. A fast and uniform photocurrent response was observed for each switch-on/off event in both graphene-TiO_2 NPs (*two-step* hydrothermal) and graphene-TiO_2 NPs-deposited electrodes under UV light (Figure S5), a response that was entirely reversible. Under UV irradiation, photocurrents of graphene-TiO_2 NPs and graphene-TiO_2 NPs (*two-step* hydrothermal) electrodes were approximately 18 and 7 times higher respectively than those of a bare anatase TiO_2 NPs electrode, which indicates that the separation efficiency of photo-induced electrons and holes was improved through the electronic interaction between graphene and TiO_2. Under a visible irradiation gap ($\lambda > 420$ nm), as expected from the results in Figure 3A, no photocurrent was recorded for both bare anatase TiO_2 NPs and graphene-TiO_2 NPs (*two-step* hydrothermal). In contrast, strong photocurrent response was observed for each switch-on/off event in the case of graphene-TiO_2 NPs, which confirms high photo-activity of graphene-TiO_2 NPs under visible light (Figure 3B)

On the basis of the above results, we tested the photocatalytic activity of graphene-TiO_2 NPs for the photodegradation of methylene blue (MB) under visible light range. **Figure 4**A shows time profile of MB absorbance spectrum observed during the incubation with graphene-TiO_2 NPs under visible light irradiation. The absorption peaks at 612 nm and 665 nm in Figure 4A correspond to dimers and monomers of MB, respectively.[23] Another peak at 619 nm corresponds to the formation of the demethylated MB during oxidative decomposition.[24] For the evaluation of degradation kinetics of MB, we measured the change of main absorption peak of MB at 665 nm, which had been widely used according to the literature.[23,25–27] While MB was slightly degraded in the presence of bare anatase TiO_2 NPs despite its high stability under visible light irradiation (Figure S6), the degradation was remarkably accelerated with graphene-TiO_2 NPs (rate constant, $k = 3.41 \times 10^{-2}$ min^{-1} at the weight ratio of 0.02:1), which was significantly higher than those of graphene-TiO_2 NPs (*two-step* hydrothermal) ($k = 4.73 \times 10^{-3}$ min^{-1}) and bare anatase TiO_2 NPs ($k = 3.28 \times 10^{-3}$ min^{-1}) (Figures 4B, S8). In addition, graphene-TiO_2 NPs performed

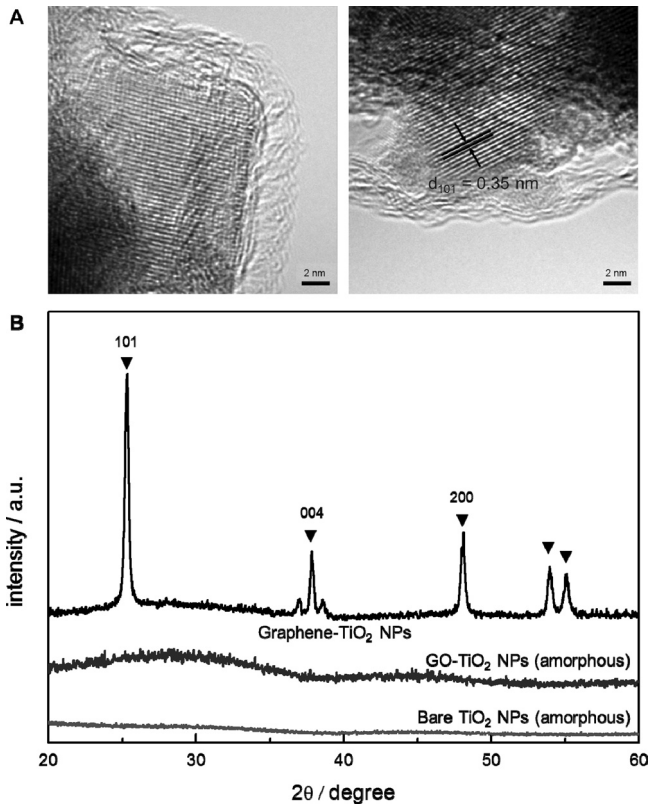

Figure 2. (A) TEM images of graphene-TiO_2 NP that shows the graphene layers on the surface of TiO_2 NP with a lattice spacing of 0.35 nm attributed to the (101) plane of anatase. The weight ratio of GO (or graphene) to TiO_2 in the GO (or graphene)-TiO_2 hybrid materials was 0.02:1. (B) X-ray diffraction patterns of bare amorphous TiO_2 NPs, GO-wrapped amorphous TiO_2 NPs, and graphene-wrapped anatase TiO_2 NPs.

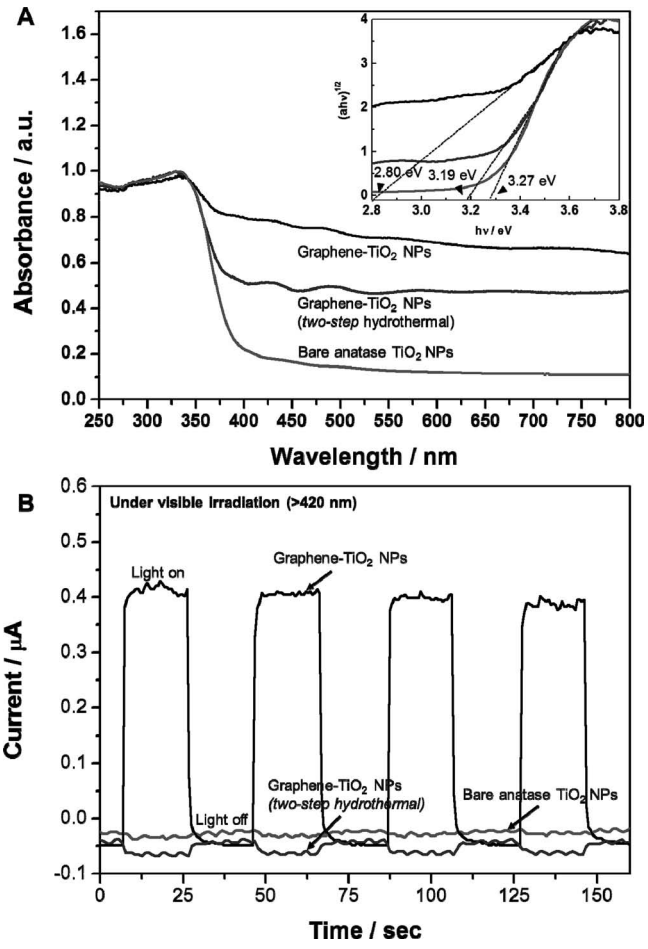

Figure 3. (A) UV-visible spectra of bare anatase TiO_2 NPs, graphene-TiO_2 NPs, and graphene-TiO_2 NPs (*two-step* hydrothermal). Note that graphene-TiO_2 NPs (*two-step* hydrothermal) were prepared first by wrapping GO nanosheets on *crystalline* anatase TiO_2 NPs, not *amorphous* TiO_2 NPs, and then reducing GO to graphene, while graphene-TiO_2 NPs were prepared by a *one-step* TiO_2 crystallization and GO reduction. The weight ratio of graphene to TiO_2 in the graphene-TiO_2 hybrid materials was 0.02:1. The inset figure shows the relationship between the transformed Kubelka-Munk function versus the light energy for each material. (B) Photocurrent responses of bare anatase TiO_2 NPs, graphene-TiO_2 NPs, and graphene-TiO_2 NPs (*two-step* hydrothermal) under visible light irradiation ($\lambda > 420$ nm).

better under visible light than Degussa P25 powders ($k = 2.63 \times 10^{-3}$ min^{-1}), a well-known commercial TiO_2–based photocatalyst (Figure S8). We attribute the significantly enhanced photocatalytic performance of graphene-TiO_2 NPs under visible light to the bandgap narrowing of the hybrid material, which should allow more absorption of visible light as well as more efficient transfer of photogenerated electrons from excited MB to TiO_2 NPs through graphene nanosheets, as illustrated in **Figure 5**. According to the literature,[28,29] the work function of excited MB, graphene, and the conduction band of bare anatase TiO_2 is –3.60, –4.40, and –4.42 eV, respectively. Since the energy level of graphene is slightly lower than the conduction band of bare anatase TiO_2, photogenerated electrons from excited MB absorbed on graphene cannot flow to the surface of TiO_2 NPs, and rapidly recombine to the ground state of MB, hindering photocatalytic activity.[29] However, the bandgap narrowing (3.2 eV → 2.8 eV) of TiO_2 in the graphene-TiO_2 NPs should change the energy level difference between graphene and TiO_2 enough to allow electrons from the excited MB to flow to the conduction band of TiO_2 NPs via graphene (*path 1* in Figure 5). Valence electrons of TiO_2 can be also excited to the conduction band state by absorbing visible light due to the sufficiently narrow bandgap of graphene-TiO_2 NPs (*path 2* in Figure 5). The excited electrons can be trapped by oxygen molecules in the aqueous solution to form singlet oxygen.[30] The reactive oxygen species generated from graphene-TiO_2 NPs can cause the oxidative decomposition of MB through demethylation process.[24] Furthermore, tightly bound graphene to TiO_2 NPs on graphene-TiO_2 NPs should promote more rapid electron transfer from the excited MB to TiO_2 via graphene nanosheets, not to the ground state of MB, hindering the recombination of excited electrons and thus accelerating visible light-driven photodegradation of MB. We further observed the effect of carbon amount in the graphene-TiO_2 NPs on the photodegradation of MB. As shown in Table S1 and Figure S7, photocatalytic efficiency was enhanced with the increasing carbon (or GO) content in the graphene-TiO_2 NPs. The increasing coverage of graphene on TiO_2 NPs with higher carbon content, as shown in

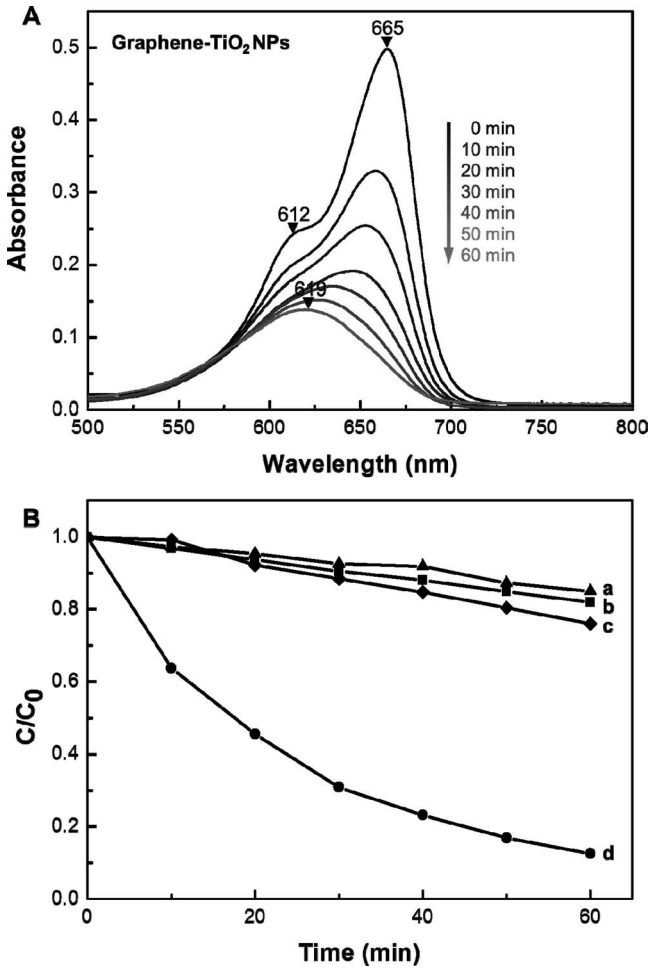

Figure 4. (A) Time profile of MB absorbance spectrum observed during incubation with graphene-TiO_2 NPs under visible light irradiation. The amount of TiO_2 was kept the same for all the samples. The degree of MB photodegradation was obtained by calculating the change of concentration (C/C_0) from the variation of absorbance (A/A_0) at 665 nm. C_0 and A_0 denote initial concentration and absorbance of MB, respectively. (B) Photodegradation of methylene blue (MB) under visible light ($\lambda > 420$ nm) by (a) P25, (b) bare anatase TiO_2 NPs, (c) graphene-TiO_2 NPs (*two-step* hydrothermal), and (d) graphene-TiO_2 NPs. The weight ratio of graphene to TiO_2 in the graphene-TiO_2 hybrid materials was 0.02:1.

Figure S2A, should facilitate faster photodegradation of MB. At the carbon content higher than 4.22 wt%, however, the photocatalytic activity of graphene-TiO_2 NPs substantially decreased due to the excess graphene not hybridized with TiO_2 NPs.

In summary, we synthesized highly photoactive graphene-wrapped anatase TiO_2 NPs through *one-step* hydrothermal GO reduction and TiO_2 crystallization from GO-wrapped amorphous TiO_2 NPs. Graphene-TiO_2 NPs exhibited a red-shift of the band-edge and a significant reduction of the bandgap (2.80 eV). We found that graphene-TiO_2 NPs possess excellent photocatalytic property under visible light for the degradation of MB with a rate constant of 3.41×10^{-2} min^{-1}, which was much higher than that of bare anatase TiO_2 NPs, graphene-TiO_2 NPs (*two-step* hydrothermal), and P25 powder. The strategy presented in this study will enable a ready integration of functional semiconductor

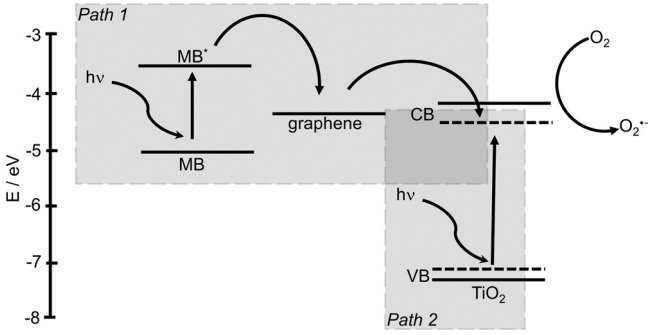

Figure 5. Suggested mechanism for the photocatalytic degradation of MB by graphene-wrapped anatase TiO_2 NPs under visible-light. The energy level of excited MB, graphene, and the conduction band of anatase TiO_2 are –3.60, –4.40, and -4.42 eV, respectively. Electrons from MB* flow to the conduction band of TiO_2 NPs via graphene (*Path 1*). Valence electrons of TiO_2 are excited to the conduction band state by absorbing visible light, which can convert oxygen molecules in the solution to singlet oxygen, the reactive oxygen species (ROSs) (*Path 2*). MB can be decomposed either by ROSs or by self-degradation under visible light irradiation. CB: conduction band, VB: valence band, MB*: excited state of MB, dotted line: intra-bandgap energy level of TiO_2 narrowed (3.2 eV → 2.8 eV) by direct interaction with Ti atoms and C atoms during the synthesis of graphene-TiO_2 NPs.

NPs and graphene nanosheets for the synthesis of highly photoactive graphene-based metal oxide hybrid materials.

Experimental Section

Materials: Hexadecylamine (HDA, 90%), KCl, titanium(IV) isopropoxide, 3-aminopropyl-trimethoxysilane (APTMS), and methylene blue (MB) were purchased from Sigma-Aldrich (St. Louis, USA). P25 was purchased from Degussa Co. (Frankfurt-Main, Germany). Graphene oxide (GO) was synthesized from graphite powder (Kropfmühl AG, Germany) according to the modified Hummers method.[31]

Synthesis of graphene-wrapped TiO_2 nanoparticles (NPs): Bare amorphous TiO_2 NPs were prepared by the sol-gel method using titanium(IV) isopropoxide as a precursor according to a previous report.[32] To wrap GO on the surface of TiO_2 NPs, TiO_2 NPs (0.4 g) were first dispersed in 200 mL ethanol by sonication for 30 min. Then, APTMS (2 mL) was added, heated, and refluxed for 4 h. APTMS-treated TiO_2 NPs were sufficiently rinsed with ethanol to wash away any remaining APTMS moiety. Different amount of negatively charged GO suspension (0.2 mg/mL) was added into positively charged amine-functionalized TiO_2 NP dispersion to change the weight ratio of GO to TiO_2 NPs (0:1, 0.0025:1, 0.005:1, 0.02:1, and 0.05:1) under vigorous stirring at pH 6. Negatively charged GO suspension (5 mL, 0.2 mg/mL) was added into positively charged amine-functionalized TiO_2 NP dispersion under vigorous stirring at pH 6. After mixing for 30 min, the mixture was centrifuged and washed with deionized water. For the crystallization of TiO_2 from amorphous to anatase phase, a hydrothermal process was used as follows. GO-TiO_2 NPs (0.4 g) were dispersed in a solution of ethanol (20 mL) and deionized water (10 mL), then autoclaved in a Teflon-lined stainless steel vessel at 180 °C for 16 h. After the hydrothermal reaction, calcination at 400 °C was carried out for 2 h in an argon atmosphere to remove organic components and obtain highly crystalline graphene-TiO_2 NPs. Graphene-TiO_2 NPs (*two-step* hydrothermal) were prepared in a *two-step* hydrothermal process: first by wrapping GO nanosheets on *crystallized* anatase TiO_2 NPs (not *amorphous* TiO_2 NPs) and then reducing GO to graphene by the same hydrothermal treatment and calcination. Bare anatase TiO_2 NPs were crystallized from bare amorphous TiO_2 NPs by hydrothermal treatment and calcination. Raman spectra in Figure S4

and XRD patterns in Figure S9 show the crystallization of amorphous TiO_2 NPs to anatase.

Photocurrent measurements: We prepared photo-electrodes by dip-coating of each NPs [i.e., bare anatase TiO_2 NPs, graphene-TiO_2 NPs, and graphene-TiO_2 NPs (*two-step* hydrothermal)] onto ITO glasses (2 cm x 1 cm). $NaSO_4$ solution (0.5 M) was used as an electrolyte. To attach NPs to ITO glass, photo-electrodes were cured at 100 °C for 1 h. After the NPs-coated ITO electrode (working electrode acting as photoanode), Ag/AgCl (reference electrode), and a platinum wire (counter electrode acting as photocathode) were connected to a WMPG1000 potentiostat/galvanostat (WonATech, Korea), an applied potential of working electrode against the counter electrode was set to 0.0 V. The photocurrent was observed for each switch-on/off event by using a xenon lamp (450 W) with a 420 nm cut-off filter.

Photocatalytic reactions: Photocatalytic activity was measured by analyzing the degradation of MB under visible light irradiation after adding the photocatalyst (8 mg) into 8 mL MB solution (2.7×10^{-2} mM). The photodegradation test was carried out by using a xenon lamp (450 W) with a 420 nm cut-off filter. The reaction mixture was stirred in the dark for 1 h to fully adsorb MB on the catalyst surface. After the confirmation of no further decrease of UV absorbance intensity caused by MB adsorption on the catalysts, the mixture was irradiated by visible light under stirring. After removing the photocatalyst from each sample by centrifugation, the degree of photodegradation was calculated by measuring the absorbance of MB at 665 nm according to the literature.[23,25–27]

Characterization: Morphology and size of NPs were observed using an S-4800 field emission scanning electron microscope (Hitachi CO., Japan) and an Tecnai F20 Transmission electron microscope (Philips Co., Netherlands) that were operated at 200 kV. Carbon content in graphene-TiO_2 NPs was analyzed by using an EA1110-FISONS elemental analyzer (ThermoQuest Italia S.P.A., Italy). The crystal structure of the TiO_2 NPs was investigated using a D/Max-2500 18 kW X-ray diffractometer (Rigaku Co., Japan) equipped with a nickel filter under scan speed of 3 °/min, Cu Kα radiation wavelength of 1.5418 Å. Absorbance spectra of bare anatase TiO_2 NPs and graphene-TiO_2 NPs were measured using a V/650 spectrophotometer (Jasco Inc., Japan) in diffuse reflectance mode. High-resolution dispersive-Raman spectra were obtained using a LabRAM HR Raman spectroscope (Horiba Co., France). Photocurrent was measured using a WMPG1000 potentiostat/galvanostat (WonATech, Korea) with a Pt counter electrode.

Supporting Information

Supporting Information is available from the WIley Online Library or from the author.

Acknowledgements

This study was supported by the National Research Laboratory (R0A-2008-000-20041-0), Global Frontier Research Program (BioDesign Center), and Converging Research Center (2009-0082276) from the National Research Foundation (NRF).

Received: October 26, 2011
Revised: December 13, 2011
Published online: January 24, 2012

[1] D. Zhang, X. Yang, J. Zhu, Y. Zhang, P. Zhang, G. Li, *J. Sol-Gel Sci. Technol.* **2011**, *58*, 594.
[2] L. Zhao, X. Chen, X. Wang, Y. Zhang, W. Wei, Y. Sun, M. Antonietti, M.-M. Titirici, *Adv. Mater.* **2010**, *22*, 3317.
[3] J. Liu, H. Bai, Y. Wang, Z. Liu, X. Zhang, D. D. Sun, *Adv. Funct. Mater.* **2010**, *20*, 4175.
[4] H. N. Kim, T. W. Kim, I. Y. Kim, S.-J. Hwang, *Adv. Funct. Mater.* **2011**, *21*, 3111.
[5] J. Du, X. Lai, N Yang, J. Zhai, D. Kisailus, F. Su, D. Wang, L. Jiang, *ACS Nano* **2011**, *5*, 590.
[6] G. Liu, Y. Zhao, C. Sun, F. Li, G. Q. Lu, H.-M. Cheng, *Angew. Chem. Int. Ed.* **2008**, *47*, 4516.
[7] A. K. Geim, K. S. Novoselov, *Nat. Mater.* **2007**, *6*, 183.
[8] A. K. Geim, *Science* **2009**, *324*, 1530.
[9] P. H. Wobkenberg, G. Eda, D-S. Leem, J. C. De Mello, D. D. C. Bradley, N. Chhowalla, T. D. Anthopoulos, *Adv. Mater.* **2011**, *23*, 1558.
[10] D. Wei, Y. Liu, *Adv. Mater.* **2011**, *22*, 3225. Li. H. Zhang, C. Fan, B. Liu, *Adv. Mater.* **2011**, *23*, 4386.
[11] L. Wang, K-Y. Pu, J. Li, X. Qi, H. Li, H. Zhang, C. Fan, B. Liu, *Adv. Mater.* **2011**, *23*, 4386.
[12] K. K. Manga, S. Wang, M. Jaiswal, Q. Bao, K. P. Loh, *Adv. Mater.* **2010**, *22*, 5265.
[13] K. Zhou, Y. Zhu, X. Yang, X. Jiang, C. Li, *New J. Chem.* **2011**, *35*, 353.
[14] J. Du, X. Lai, N. Yang, J. Zhai, D. Kisailus, F. Su, D. Wang, L. Jiang, *ACS Nano* **2011**, *5*, 590.
[15] H. Zhang, X. Lv, Y. Li, Y. Wang, J. Li, *ACS Nano* **2010**, *4*, 380.
[16] Y. Hau NG, I. V. Lightcap, K. Goodwin, M. Matsumura, P. V. Kamat, *J. Phys, Chem. Lett* **2010**, *1*, 2222.
[17] W. F. Zhang, Y. L. He, M. S. Zhang, Z. Yin, Q. Chen, *J. Phys. D: Appl. Phys.* **2000**, *33*, 912.
[18] C. Gomez-Navarro, R. Thomas Weitz, A. M. Bittner, M. Scolari, A. Mews, M. Burghard, K. Kern, *Nano Lett.* **2007**, *7*, 3499.
[19] D. Reyes-Coronado, G. Rodrıguez-Gattorno, M. E. Espinosa-Pesqueira, C. Cab, R. Coss, G. Oskam, *Nanotechnology* **2008**, *19*, 145605.
[20] K. Yanagisawa, J. Ovenstone, *J. Phys. Chem. B* **1999**, *103*, 7781.
[21] C. Nethravathi, M. Rajamathi, *Carbon* **2008**, *46*, 1994.
[22] H. Zhang, X. Lv, Y. Li, Y. Wang, J. Li, *ACS Nano* **2010**, *4*, 380.
[23] C. An, S. Peng, Y. Sun, *Adv. Mater.* **2010**, *22*, 2570.
[24] T. Zhang, T. Oyama, A. Aoshima, H. Hidaka, J. Zhao, N. Serpone, *J. Photochem. Photobiol. A* **2001**, *140*, 163.
[25] S. S. Soni, M. J. Henderson, J.-F. Bardeau, A. Gibaud, *Adv. Mater.* **2008**, *20*, 1493.
[26] E. Elmalem, A. E. Sauders, R. Costi, A. Salant, U. Banin, *Adv. Mater.* **2008**, *20*, 4312.
[27] X. Qiu, Y. Zhao, C. Burda, *Adv. Mater.* **2007**, *19*, 3995.
[28] Y. S. Ocak, M. Kulakci, T. Kilicoglu, R. Turan, K. Akkilic, *Synt. Met.* **2009**, *159*, 1603.
[29] J. Zhang, Z. Xiong, X. S. Zhao, *J. Mater. Chem.* **2011**, *21*, 3634.
[30] Z. Xiong, L. L. Zhang, X. S. Zhao, *Chem. Eur. J.* **2011**, *17*, 2428.
[31] Y. X. Xu, H. Bai, G. W. Lu, C. Li, G. Q. Shi, *J. Am. Chem. Soc.* **2008**, *130*, 5856.
[32] D. H. Chen, F. Z. Huang, Y. B. Cheng, R. A. Caruso, *Adv. Mater.* **2009**, *21*, 2206.